



The language-related cerebro-cerebellar pathway in humans: a diffusion imaging–based tractographic study

Hu Yin^{1,2}, Fangrong Zong³, Xiaofeng Deng^{1,2}, Dong Zhang^{1,2}, Yan Zhang^{1,2}, Shuo Wang^{1,2}, Yu Wang^{2,4}, Jizong Zhao^{1,2}

¹Department of Neurosurgery, Beijing Tiantan Hospital, Capital Medical University, Beijing, China; ²China National Clinical Research Center for Neurological Diseases, Beijing, China; ³School of Artificial Intelligence, Beijing University of Posts and Telecommunications, Beijing, China; ⁴Department of Neurology, Beijing Tiantan Hospital, Capital Medical University, Beijing, China

Contributions: (I) Conception and design: H Yin, F Zong; (II) Administrative support: J Zhao; (III) Provision of study materials or patients: Y Zhang, D Zhang, S Wang; (IV) Collection and assembly of data: X Deng, Y Wang; (V) Data analysis and interpretation: H Yin, F Zong, J Zhao; (VI) Manuscript writing: All authors; (VII) Final approval of manuscript: All authors.

Correspondence to: Prof. Jizong Zhao. Department of Neurosurgery, Beijing Tiantan Hospital, Capital Medical University, No. 119 South 4th Ring West Road, Fengtai District, Beijing 100070, China. Email: zhaojizong@bjtth.org; Prof. Fangrong Zong. School of Artificial Intelligence, Beijing University of Posts and Telecommunications, 10 Xitucheng Road, Haidian District, Beijing 100876, China. Email: Fangrong.zong@bupt.edu.cn.

Background: The cerebellum and cerebral cortex form the most important cortico-cerebellar system in the brain. However, diffusion magnetic resonance imaging (MRI)-based tractography of the connecting white matter between the cerebellum and cerebral cortex, which support language function, has not been extensively reported on. This work aims to serve as a guideline for facilitating the analysis of white matter tracts along the language-related cerebro-cerebellar pathway (LRCCP), which includes the corticopontine, pontocerebellar, corticorubral, rubroolivary, olivocerebellar, and dentatorubrothalamic tracts.

Methods: The LRCCP templates were developed via processing the high-resolution, population-averaged atlas available in the Human Connectome Project (HCP)-1065 dataset (2017 Q4, 1,200-subject release) in DSI Studio. The deterministic tracking was performed with the manually selected regions of interest (ROIs) on this atlas according to prior anatomic knowledge. Templates were then applied to the MRI datasets of 30 health participants acquired from a single hospital to verify the practicability of the tracking. The diffusion tensor and shape analysis metrics were calculated for all LRCCP tracts. Differences in the tracking metrics between the left and right hemispheres were compared, and the related white matter asymmetry was discussed.

Results: The LRCCP templates were successfully created and applied to healthy participants for quantitative analysis. Significantly higher mean fractional anisotropy (FA) values were discovered on the left (L) corticorubral tract [L, 0.43 ± 0.02 vs. right (R), 0.41 ± 0.02 ; $P < 0.01$] and left dentatorubrothalamic tract (L, 0.47 ± 0.02 vs. R, 0.46 ± 0.02 ; $P < 0.01$). Significant differences in tract volume and streamline number were observed between the corticopontine, corticorubral, and dentatorubrothalamic tracts. The size of the right corticopontine and corticorubral tracts were smaller, and both had smaller streamline numbers and innervation areas when compared with the contralateral sides. The R dentatorubrothalamic tract showed a larger volume (R, $23,582.47 \pm 4,160.71$ mm³ vs. L, $19,821.27 \pm 2,983.91$ mm³; $P < 0.01$) and innervation area (R, $2,117.37 \pm 433.98$ mm² vs. L, $1,610.00 \pm 356.19$ mm²; $P < 0.01$) than did the L side. No significant differences were observed in the rubroolivary tracts.

Conclusions: This work suggests the feasibility of applying tractography templates of the LRCCP to quantitatively evaluate white matter properties associated with language function. Lateralized diffusion metrics were observed in preliminary experiments. LRCCP tractography-based research may provide a potential quantitative method to better understanding neuroplasticity.

Keywords: Diffusion magnetic resonance imaging; white matter asymmetry; tractography; cerebellum; language; shape analysis

Submitted Apr 01, 2022. Accepted for publication Nov 27, 2022. Published online Feb 10, 2023.

doi: 10.21037/qims-22-303

View this article at: <https://dx.doi.org/10.21037/qims-22-303>

Introduction

In recent decades, it has been realized that, in addition to being an auxiliary part of the human brain that regulates and coordinates motor function, the cerebellum is also involved in language processing (1-6). Since the 19th century, the cerebellum has been shown to play an important role in nonmotor language functions, including word generation and phonologic and semantic processing (7-10). Leiner *et al.* were the first to discover the neural connection between the cerebellum and the nonmotor cortex, especially in the prefrontal area (11,12). From the perspective of central nervous system evolution, the lateral portion of the cerebellum and the dentate nucleus exhibit a disproportionately enlarged volume. The related cerebral cortex region also shows the same expansion (11,13). These connected areas form the cortico-cerebellar system. Evidence from neuroanatomy, functional magnetic resonance imaging (fMRI), and viral-tract tracing studies has verified such connections between the cerebral cortex and cerebellum (14-18).

The cerebro-cerebellar pathway mainly consists of a descending pathway and an ascending pathway (*Figure 1*) (4,19). The first part of the descending pathway consists of corticopontine tracts and the pontocerebellar tracts (20,21). Fibers originate from various parts of the cerebral cortex, pass through the internal capsule, and end at the unilateral pontine nucleus. The pontocerebellar tracts enter the cerebellum via the middle cerebellar peduncle. The second part of the descending pathway consists of the corticorubral, rubroolivary, and olivocerebellar tracts. The corticorubral tracts originate from the cerebral cortex and extend to the red nucleus (RN). The rubroolivary tracts contain a cell body in the RN with axons reaching the inferior olivary nucleus (ION) (3,12). The olivocerebellar tracts from the ION navigate a complex path to the cerebellum, and thus more detail on this is provided further below. The ascending pathway is also known as the dentatorubrothalamic tract (DRTT). It originates from the unilateral dentate nucleus and ascends through the superior cerebellum peduncle. Before it ending at the RN, a part of

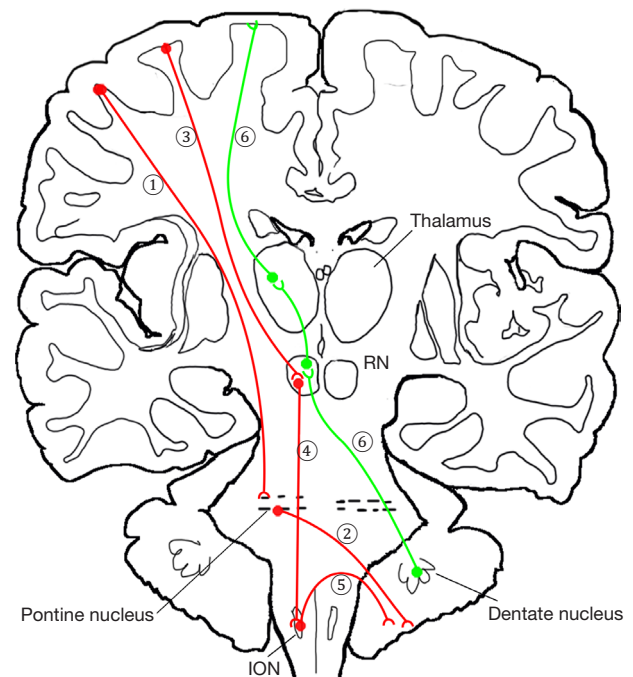


Figure 1 Diagram of the language-related cerebro-cerebellar pathway. Lines in red depict the descending pathway from the cortex to the cerebellum. Green lines depict the ascending pathways. ① corticopontine tract; ② pontocerebellar tract; ③ corticorubral tract; ④ rubroolivary tract; ⑤ olivocerebellar tract; ⑥ dentatorubrothalamic tract. ION, inferior olivary nucleus; RN, red nucleus.

the fiber bundle crosses the midline to join the contralateral dentatorubrothalamic tract. The other part of the fiber bundle directly passes through the RN to the thalamus (22).

The mechanism by which the cerebellum is involved in language function is not yet been fully understood (2,4). It is well accepted that language-related information is transmitted via cerebro-cerebellar circuits. Researchers have observed improvements in some language domains after direct electrical stimulation (DES) of the cerebellum, suggesting that there is a potential for language recovery by neuromodulation in the cerebellum. As a novel, noninvasive,

neuroimaging technique used to map white matter pathways *in vivo*, diffusion tensor imaging (DTI) has been widely used in the dissections of white matter fiber bundles via the measurement of anisotropic diffusion (23,24). Unlike the arcuate tract and superior longitudinal tract, which have been frequently noted to play an important role in brain language function, the quantitative analysis of the language-related cerebro-cerebellar pathway (LRCCP) has only sparsely been reported on (25-28). One possible reason is the LRCCP template or atlas is unavailable for group analysis, as brainstem-related tractography is more challenging than is cerebrum-related tractography.

To mitigate this problem, this study aimed to provide a new tractography template of the cerebro-cerebellar pathway to comprehensively investigate language function. The high-resolution Human Connectome Project (HCP) datasets (29,30) were used to construct the diffusion MRI-based template. Furthermore, the feasibility of applying the created template to datasets with clinical quality was evaluated by applying the template to automatically track the LRCCP in healthy participants. Using this new LRCCP template, we quantified the shape parameters of the unique pathway and investigated the white matter asymmetry in healthy participants (31). This article is presented in accordance with the STROBE reporting checklist (available at <https://qims.amegroups.com/article/view/10.21037/qims-22-303/rc>).

Methods

Creation of the tractography template

A total of 11 tracts are included in the cerebro-cerebellar pathway: (I) the corticopontine tracts [left (L) and right (R)], (II) the pontocerebellar tracts, (III) the corticorubral tracts (L and R), (IV) the rubroolivary tracts (L and R), (V) the olivocerebellar tracts (L and R), and (VI) the DRTTs (L and R). There is no direct connection between the cerebrum and the cerebellum; therefore, direct end-to-end fiber tracking could not be applied to the LRCCP. The strategy we proposed was to track the 11 direct connections separately and unite them as a complete template using DSI Studio software (<http://dsi-studio.labsolver.org/>) via atlas-guided tracking recognition (32). Two (the dentatorubrothalamic and pontocerebellar tracts) of the six direct connections were already available in the DSI studio tract template list. For those not included in the built-in list, the templates were

developed via processing the high-resolution population-averaged atlas.

The HCP 1065 template was constructed from the diffusion MRI data of 1,065 participants in the HCP (2017 Q4, 1200-subject release; females, 575; males, 490; age range, 22–37 years; mean age, 28.74 years). A multishell diffusion scheme was used, with b-values of 1,000, 2,000, and 3,000 s/mm², respectively; and diffusion sampling direction numbers of 90, 90, and 90, respectively. The isotropic resolution of the image was 1.25 mm³. The diffusion data were reconstructed in the Montreal Neurological Institute (MNI) space using q-space diffeomorphic reconstruction (33) to obtain the spin distribution function (34). A diffusion sampling length ratio of 1.7 was used, and the output resolution was 1 mm.

The seed region of interest (ROI), region of avoidance (ROA), and end/terminate region were set on the HCP 1065 template based on knowledge of anatomy, as below:

- (I) Corticopontine tracts: all components of the 4 parts (frontal, temporal, occipital, and temporal) of the cerebral cortex lobe were included in the DSI studio tract template list and were merged to form the corticopontine tracts.
- (II) Pontocerebellar tracts: these acts were already present in the DSI studio tract template list, and thus the software default template was applied.
- (III) Corticorubral tract: the RN was set as an ROI to narrow down the “reticular tracts” in the DSI studio tract template list, the built-in atlas then detected the corticorubral tracts as part of the “Reticular tract”, and finally, the fibers at the distal end of the RN were manually terminated.
- (IV) Rubroolivary tracts: the ION was manually drawn in the fractional anisotropy (FA) color map, the RN was set as both a seed region and terminative region, and the ION was set as an ROI.
- (V) Olivocerebellar tracts: the ION was set as the seed point, and the contralateral cerebellum was set as a terminate region instead of the contralateral cerebellar cortex because the climbing fibers usually sprout collateral branches before reaching the cerebellar cortex; the pontine was defined as a ROA to ensure that fibers originating from the ION passed through the contralateral inferior cerebellar peduncle (ICP) and finally ended at the contralateral cerebellum; a horizontal plane right upon the ION was additionally set as an ROA to rule out longitudinal fibers, and another 2 horizontal planes

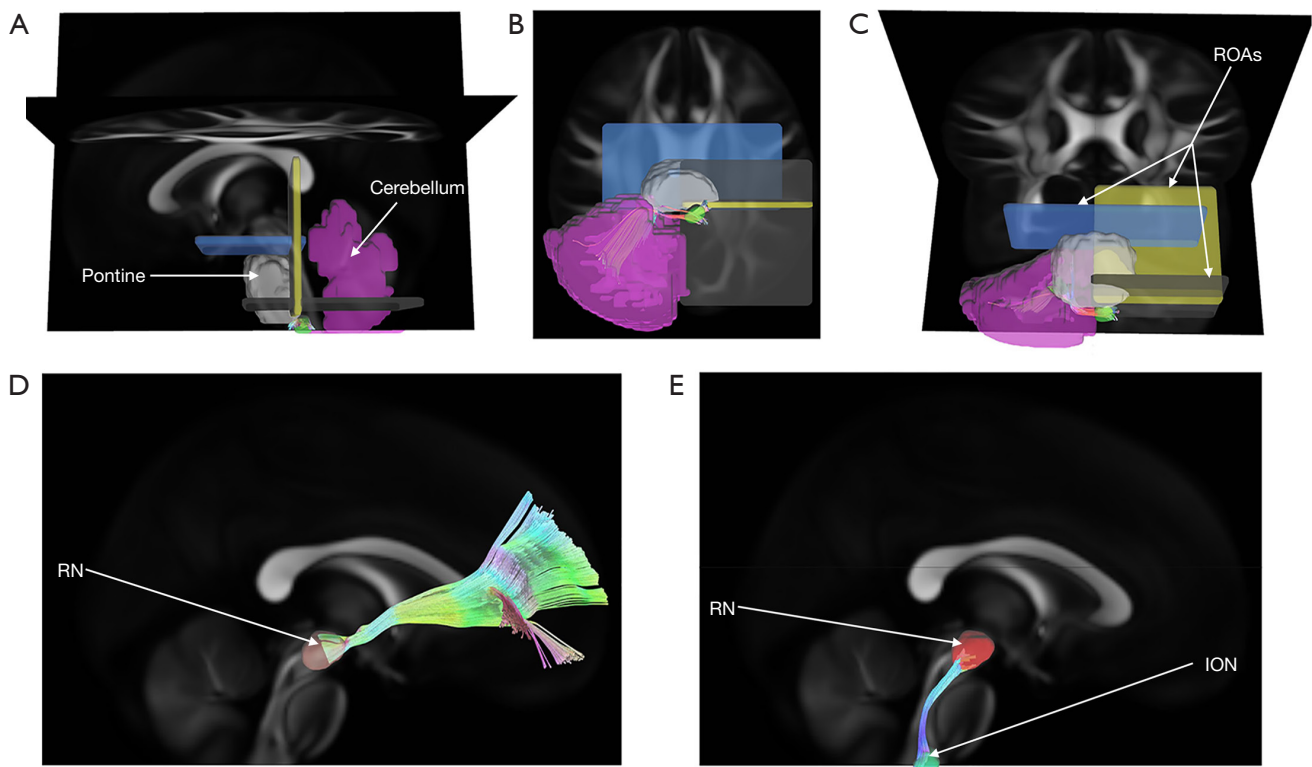


Figure 2 Illustration of the tracking strategy of the olivocerebellar, rubroolivary, and corticorubral tracts. (A–C) The position of 3 ROAs (blue, yellow, and black), seed region (green), and terminative region (dark red) in the olivocerebellar tract, respectively. (D) The position of the seed region (light red) and terminative region (green) in the rubroolivary tract. (E) The position of the ROI in the corticorubral tract. ROA, region of avoidance; RN, red nucleus; ION, inferior olivary nucleus.

upon the pontine and a vertical plane in the posterior part of the pontine were set as ROAs (*Figure 2*); the RN and unilateral cerebellum were loaded from the built-in region list in the DSI studio; the pontine was drawn to cover all pontine nucleus regions, and the ION was drawn on both sides separated by the middle line in the fusiform.

After setting the tracking-related regions as defined above, the deterministic fiber tracking algorithm (32) was used to create the templates. The tracking parameters were applied as follows: anisotropy threshold, 0.07208; angular threshold, 45 degrees (except for the olivocerebellar tractography, which was 90 degrees); and, step size, 0.5 mm. The fiber trajectories were smoothed by averaging the propagation direction with a percentage of the previous direction. The percentage was randomly selected from 0% to 95%. Tracks with a length shorter than 15 mm or longer than 300 mm were discarded. A total of 500,000 seeds were placed, and topology-informed pruning (35) was applied to the

tractography with 16 iteration(s) to remove false connections.

After all the 11 newly built tract templates were obtained, they were integrated with the prior existing tract templates to form the new tractography atlas (*Figure 3*).

Study participants

This observational study was conducted in accordance with the Declaration of Helsinki (as revised in 2013), approved by the Institutional Review Board of Beijing Tiantan Hospital (No. KY2018-103-01), and registered in the Chinese Trial Registry (clinical trial No. ChiCTR1900020993). All healthy participants were recruited via advertisements from local communities and colleges (36). Written informed consent was obtained from the participants who were all enrolled between January 2018 and November 2020. The inclusion criteria for participants were as follows: (I) right-handedness confirmed by the Edinburgh handedness inventory, (II) native Mandarin Chinese speakers, (III) age

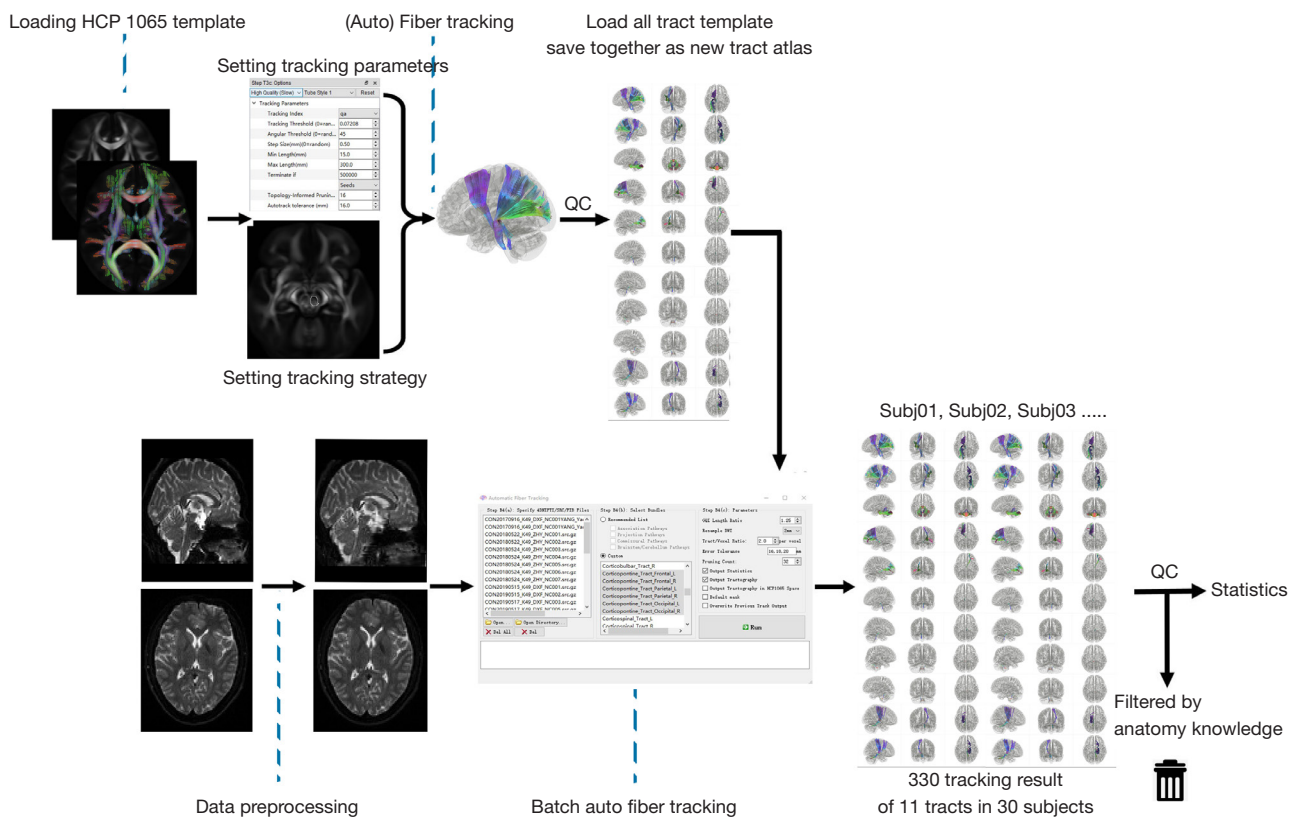


Figure 3 Workflow of creation of tract templates and application in healthy participants. This figure briefly shows the workflow of the current study, including making the required tract templates and merging them into an existing template set, and then running them on normal participant data. A quality check was conducted by loading the B0 image and FA color maps after the templates were generated to check whether the position and relationship between the path and surrounding structures were in line with anatomical knowledge. HCP, Human Connectome Project; QC, quality control; Subj, subject; FA, fractional anisotropy.

of 18 to 60 years, and (IV) high school educational level or above. Participants were excluded if they had neurological or psychiatric conditions.

Diffusion MRI data acquisition

The MRI data were derived from our previously published study. Data preprocessing was consistent with that reported before (36). The diffusion MRI scan was performed on a 3-T Prisma-fit scanner (Siemens Healthineers, Erlangen, Germany) with a 20-element head-neck coil. A fully sampled spin-echo echo-planar imaging was acquired for the diffusion dataset (1.5 mm isotropic resolution, repetition time = 8,100 ms, echo time = 75 ms, matrix = 100×100×72). We acquired 3 frames with $b = 0$ s/mm² and 64 frames along isotropically distributed diffusion directions with $b = 1,000$ s/mm². The total acquisition time for the

diffusion MRI study was approximately 9 minutes for each participant. In addition, a T1-weighted, magnetization-prepared, rapid-acquisition gradient-echo sequence was also applied (repetition time = 2,530 ms, echo time = 3.37 ms, flip angle = 7°, field of view = 256×256 mm², matrix = 256×256, voxel size = 1.0 × 1.0 × 1.0 mm³, and number of slices = 176).

Diffusion MRI data processing

Before the tractography process, the diffusion MRI data were first visually inspected for major artifacts. Then, data preprocessing mainly consisting of correcting artifacts, such as eddy current, subject head movement, and field inhomogeneity effects, was performed. The eddy current-induced field inhomogeneity and the head motion for each image volume were corrected using the Eddy function in

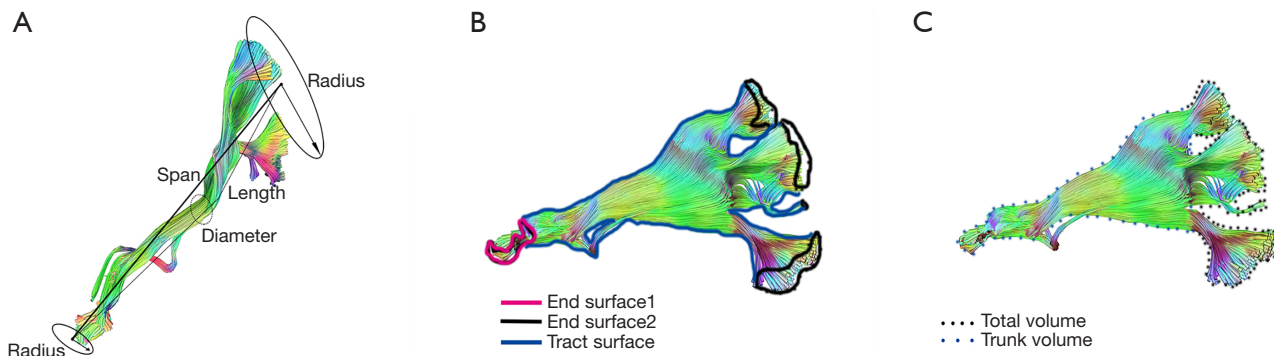


Figure 4 Shape analyses of a fiber bundle in healthy participants. The diagram shows shape metrics in the shape analysis.

the Functional Magnetic Resonance Imaging of the Brain (FMRIB) Software Library (FSL; <https://fsl.fmrib.ox.ac.uk/fsl/fslwiki/eddy>) and was followed by correction for gradient nonlinearity. To decrease spatial intensity inhomogeneity as raised by the excitation field, bias field correction was conducted on the b_0 image ($b=0$ s/mm²) and subsequently applied to all diffusion-weighted images.

After the artifacts were corrected, the reconstruction was conducted using the generalized q-sampling imaging (GQI) method (33). The diffusion sampling length ratio was 1.25. A second inspection was applied for image quality, and then the mask before reconstruction was started. In the automatic fiber tracking process, the option of output statics and output tractography were checked to ensure a subsequent quality inspection could be conducted. Diffusion metrics, including mean FA, mean diffusivity (MD), axial diffusivity (AD), and radial diffusivity (RD), were then calculated in the outputted statistical results (24).

Tractography using the new template in healthy participants

After all of the 11 tract templates were integrated with the prior existing tract templates, batch auto fiber tracking was conducted. A deterministic fiber tracking algorithm (32) was used with augmented tracking strategies (31) to improve reproducibility. The anatomy before a tractography atlas (30) was used to map each included tract with a distance tolerance of 16 mm. A seeding region was placed at the track region indicated by the tractography atlas. A ROA was placed at the track tolerance region. The track-to-voxel ratio was set to 2. The angular threshold was randomly selected in the range of 15–90 degrees. The step size was randomly selected in the range of 0.5–1.5 voxels.

Tracks with a length shorter than 30 or longer than 300 mm were discarded. Topology-informed pruning (35) was applied to the tractography, with 32 iteration(s) undertaken to remove false connections.

Shape analysis

The shape analysis algorithm of the white matter tract was first introduced by Yeh (31). The present study was conducted by using an automatic analysis package integrated into the DSI Studio software. The shape analysis metrics (*Figure 4*) included mean length, span, curl, elongation, diameter, volume, total surface area, total radius of end regions, total area of end regions, irregularity, area of end regions, radius of end region, and irregularity of end region. The detailed definitions of these diffusion and shape parameters are contained in the references of Mori *et al.* (24) and Yeh (31), and will not be described in this paper.

Statistical analysis

The data of results were analyzed using SAS v. 9.4 (SAS Institute, Cary, NC, USA) software. The paired *t*-test or Wilcoxon rank-sum test was performed for differences between the tracts of the left and right sides in all metrics. A *P* value <0.05 was considered statistically significant. In addition, the lateralization index (LI) was calculated for interest metrics. The LI was calculated according to the following formula: $LI = (L - R)/(L + R)$ (9,37-39).

Results

Demographic data

A total of 30 healthy participants were finally enrolled.

The mean age was 29.67 ± 10.14 years, and 14 (46.7%) were males. They were all native speakers and right-handed as confirmed by the Edinburgh handedness inventory.

The tractography template of LRCCP and application in healthy participants

All 11 tract templates were successfully created and saved into a new tractography template using the HCP 1065 population-averaged datasets (Figure 5). Templates of brainstem-related tracts were achieved without false positives or missing streamlines or false pathways although complicated crossing patterns and limitations of spatial resolution were present. A deterministic fiber tracking algorithm was applied to obtain the 11 tract results in the 30 healthy participants. A total of 330 tractography results were visually inspected for possible errors. The olivocerebellar tracts in all participants were discarded because they were inconsistent with the anatomical evidence (L and R). We finally verified 9 out of 11 tract templates with a 100% positive tracking rate and no false positive fibers in the datasets of our healthy participants.

Quantitative analyses of the LRCCP

The output of statics included 2 main parts: diffusion metrics and shape metrics. All the results of these parameters in 30 healthy participants are shown in Table 1 and Table 2 (the pontocerebellar tracts data are provided in Supplementary Table 1). As can be seen from Table 1, the corticopontine tracts show the highest mean FA value and are followed by the DRTTs, while the pontocerebellar tracts own the lowest mean FA value. It seems that tracts with an inferior position tend to show a relatively lower mean FA value. Comparison between the L and R tracts showed a significant difference in the mean FA in the corticorubral tracts and the DRTTs. Higher mean FA values were evident on the L side for both tracts.

For shape analysis metrics, differences in tract volume, streamline number, and area of endpoint 1 were observed in the corticopontine tract, corticorubral tract, and DRTT. The size of the R corticopontine tract and the R corticorubral tract were smaller, and both had smaller streamline numbers and innervation areas compared with the contralateral tracts. For DRTT, the result was the opposite. The R DRTT had a larger volume and streamline number. The innervation area was also larger than that of the L side. No difference was observed in the rubroolivary

tracts.

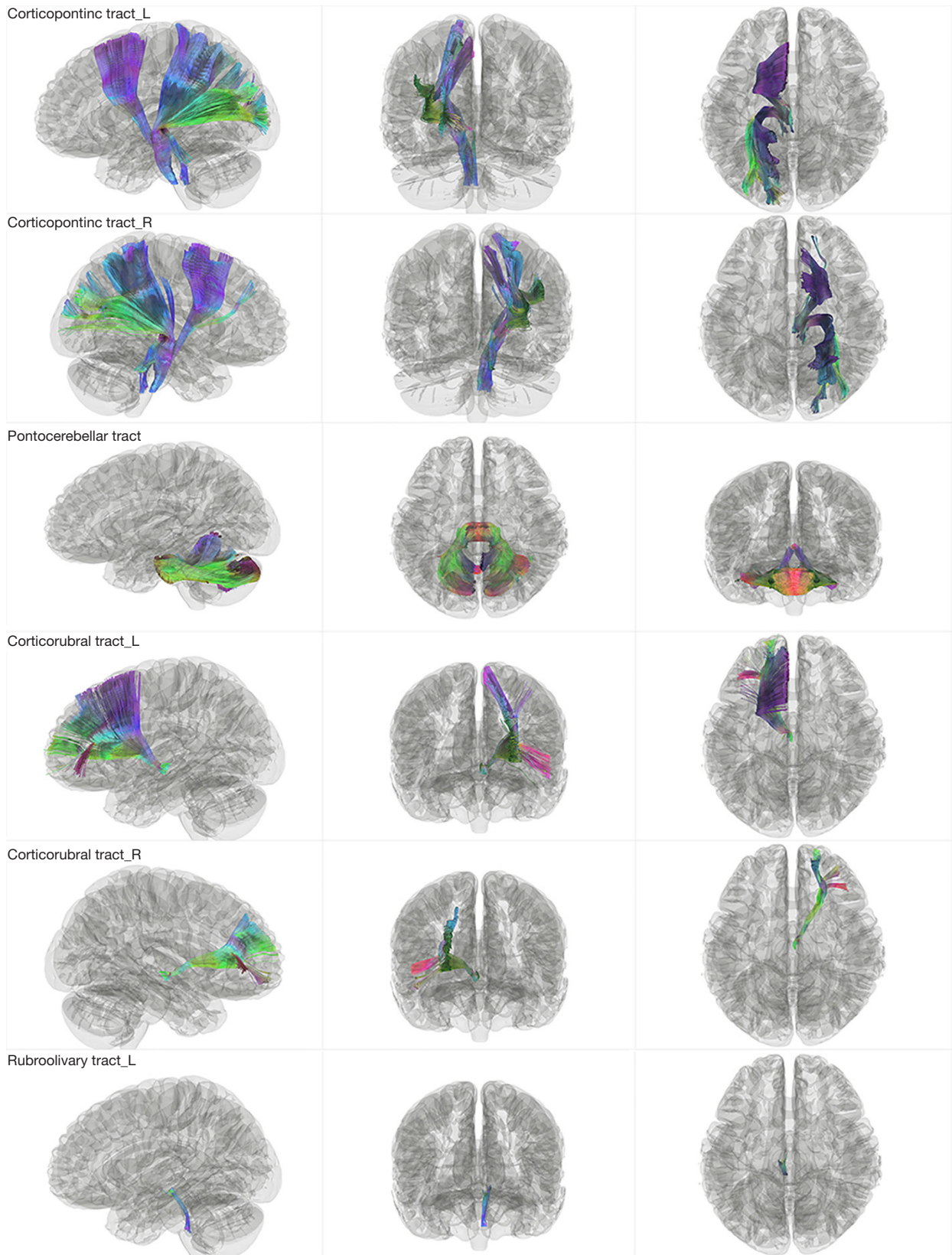
The results of LI are almost consistent with the above-mentioned result (Figure 6). The corticorubral tracts tend to be leftward lateralized for the reason that there were 93.33%, 90.00%, and 80.00% of participants with $LI > 0.2$ for streamline number, volume, and area of the end region 1. The DRTTs tend to be rightward lateralized with 93.33%, 80.00%, 80.00%, and 93.33% of participants with $LI < 0$ for streamline number, diameter, volume, and area of the end region 1. As for the corticopontine tracts and rubroolivary tracts, no consistent lateralization pattern was observed in the different metrics.

Discussion

We created a set of tractography templates of LRCCP from the HCP datasets. These tract templates worked well with the datasets of our participants, except for the olivocerebellar tracts. The diffusion metrics and shape analysis metrics of the LRCCP were calculated, and the white matter asymmetry was analyzed. Results showed that differences were present between the L and R sides in various aspects. The leftward lateralization pattern seemed more common and robust than did the rightward lateralization. A mixed situation was observed in the LRCCP. The method in our study provided a comprehensive and quantitative evaluation system for the LRCCP and allowed for the accurate capture of imperceptible white matter changes in the processes of neural function.

The particularity of the olivocerebellar tracts

The results of both olivocerebellar tracts failed to reflect the anatomical facts in almost every participant. We tried to interpret the result from several aspects. First, the olivocerebellar tracts originate from the ION traveling first across the midline and finally joining the contralateral ICP before entering the cerebellum, thus forming cross fibers in this region (40-44). The olivocerebellar tracts pass through the restiform body where the spinocerebellar tract is located, with both running laterally to trigeminal nerve branches to enter the ICP (44,45). It is difficult to separate the olivocerebellar tracts due to the parallel fibers and complex adjacent relationships (46,47). Furthermore, the brainstem, especially the pontine, has several disadvantages for fiber tracking: a small volume, complex fiber-crossing situations, and motion artefacts (48). Finally, the topology-informed pruning (TIP) algorithm must be mentioned (35).



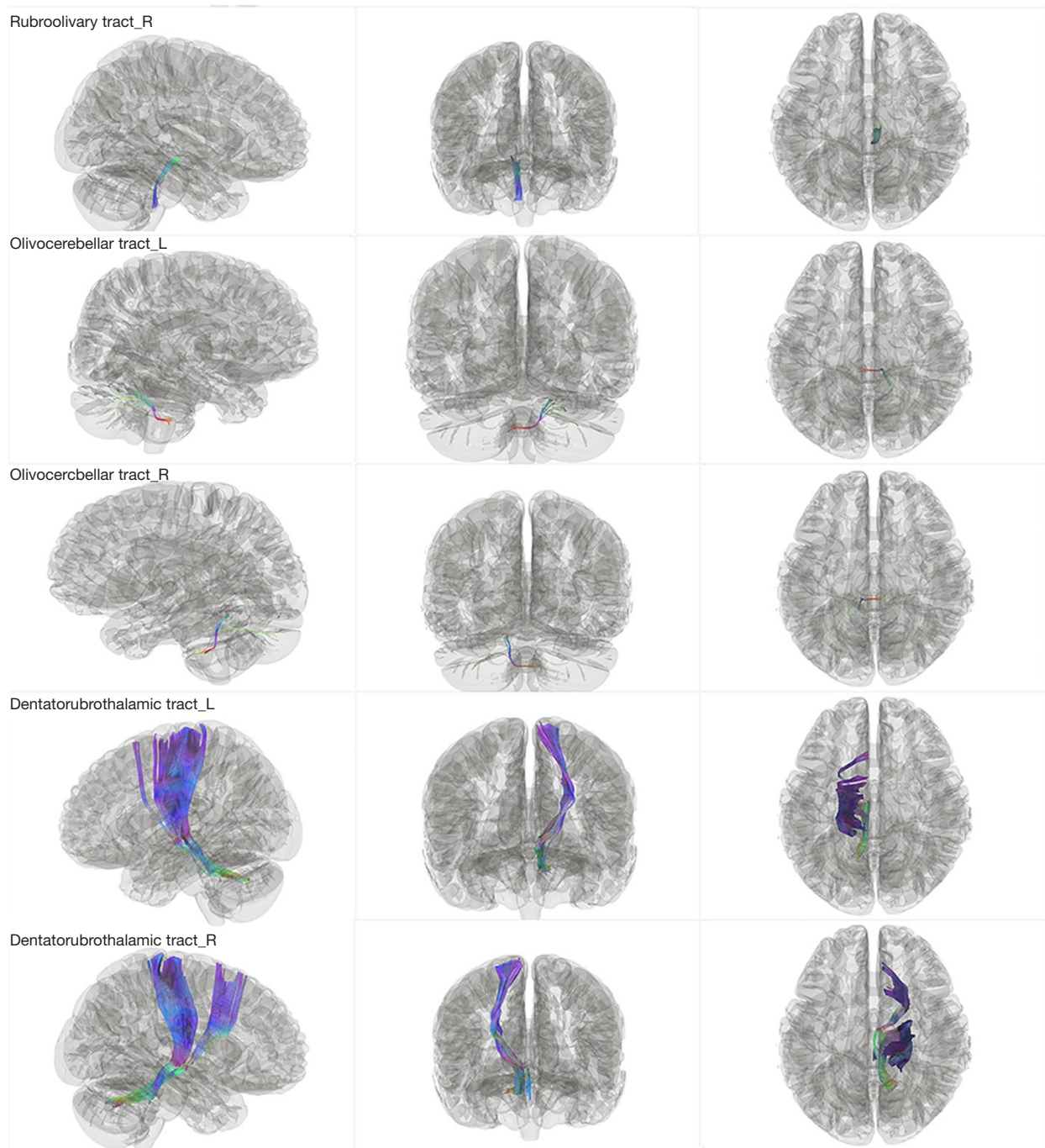


Figure 5 The template of the LRCCP. All 11 tract templates were made from the HCP 1065 (1 mm) datasets. The pontocerebellar tracts could not be separated into a left part and a right part due to the tractography limitation. LRCCP, language-related cerebro-cerebellar pathway; HCP, Human Connectome Project; L, left; R, right.

Table 1 Quantitative results of diffusion and shape metrics of the corticopontine and dentatorubrothalamic tracts

Parameters	Corticopontine tract			Dentatorubrothalamic tract		
	Left	Right	P value	Left	Right	P value
Number of streamlines	24,369.43 ±3 270.81	22,979.27±2,982.78	0.03	8,580.10±1,617.08	10,870.83±1,893.72	<0.01
Mean length (mm)	135.29±6.04	131.98±6.08	<0.01	128.14±5.79	123.07±5.00	<0.01
Span (mm)	52.86±3.05	53.11±2.51	0.55	51.52±2.23	50.36±2.08	<0.01
Curl	2.56±0.09	2.49±0.09	<0.01	2.49±0.07	2.45±0.07	<0.01
Elongation	6.59±0.45	7.07±0.53	<0.01	9.20±0.78	7.97±0.78	<0.01
Diameter (mm)	20.60±1.13	18.73±1.06	<0.01	14.00±1.04	15.56±1.35	<0.01
Volume (mm ³)	45,235.90±5,487.85	36,470.9±4,429.69	<0.01	19,821.27±2,983.91	23,582.47±4,160.71	<0.01
Trunk volume (mm ³)	22,594.13±6,852.77	21,732.77±4,546.82	0.70	13,881.23±4,157.64	11,154.17±3,541.53	<0.01
Branch volume (mm ³)	22,641.77±8,246.18	14,738.13±4,287.68	<0.01	5,940.03±3,487.57	12,428.30±3,012.40	<0.01
Total surface area (mm ²)	85,972.80±9,514.47	70,252.33±8,228.04	<0.01	36,408.03±4,637.10	43,830.10±6,611.73	<0.01
Total radius of ER (mm ²)	37.61±5.56	28.65±3.20	<0.01	16.34±1.38	21.66±2.77	<0.01
Total area of ER (mm ²)	5,886.60±814.49	5,184.17±645.75	<0.01	2,006.33±412.01	2,606.37±530.03	<0.01
Irregularity	9.80±0.62	9.03±0.63	<0.01	6.44±0.36	7.25±0.50	<0.01
Area of ER 1 (mm ²)	4,591.97±748.41	4,060.43±603.34	<0.01	1,610.00±356.19	2,117.37±433.98	<0.01
Radius of ER 1 (mm)	26.61±3.68	19.02±2.77	<0.01	9.90±1.18	14.07±2.23	<0.01
Irregularity of ER 1	0.50±0.14	0.29±0.10	<0.01	0.20±0.05	0.31±0.10	<0.01
QA	0.20±0.02	0.19±0.02	<0.01	0.18±0.02	0.17±0.02	<0.01
NQA	0.35±0.02	0.34±0.02	<0.01	0.32±0.02	0.31±0.01	<0.01
FA	0.50±0.02	0.50±0.02	0.21	0.47±0.02	0.46±0.02	<0.01
MD	0.87±0.03	0.86±0.03	0.65	0.93±0.04	0.91±0.04	<0.01
AD	1.38±0.04	1.37±0.03	0.68	1.39±0.04	1.36±0.05	<0.01
RD	0.61±0.04	0.61±0.04	0.88	0.70±0.04	0.68±0.04	0.12

Data are shown as mean ± standard deviation. P<0.05 is considered statistically significant. ER, end region; QA, quantitative anisotropy; NQA, normalized quantitative anisotropy; FA, fractional anisotropy; MD, mean diffusivity; AD, axial diffusivity; RD, radial diffusivity.

The probability that the TIP algorithm considers a fiber bundle as “false” increases substantially as its size decreases (30). Given the volume of the olivocerebellar tract was much smaller than that of other tracts, the tract had a higher probability of being determined as the “false fiber”. All of the aforementioned factors made the fiber tracking procedure in these areas challenging. To mitigate this problem, a high-resolution image and a longer scan time may be required in future studies (49,50). The imaging quality of the *in vivo* brainstem and cerebellum could be improved to more successfully obtain data on the olivocerebellar tracts (43).

Tracking strategy

Anatomical knowledge can better guarantee fiber tracking is undertaken correctly (51). The tracking strategy and the visual quality check of the tract template results were conducted according to the anatomical knowledge of the researchers in our study. The dentatorubrothalamic, pontocerebellar, and corticopontine tracts from different lobes were already present in the built-in tracking list of the DSI studio, and its accuracy and practicality have been proven. To analyze the corticopontine tracts as a whole, they were merged in the newly created LRCCP template.

Table 2 Quantitative results of diffusion and shape metrics of the rubroolivary and corticorubral tracts

Parameters	Rubroolivary tract			Corticorubral tract		
	Left	Right	P value	Left	Right	P value
Number of streamlines	805.47±163.48	796.97±201.14	0.76	11,302.3±2,173.21	5,041.53±1,006.13	<0.01
Mean length (mm)	44.3±4.62	44.71±5.79	0.61	99.9±4.43	97.58±6.17	0.01
Span (mm)	18±1.73	18.08±2.07	0.81	40.65±1.73	40.63±3.08	0.9
Curl	2.46±0.13	2.47±0.14	0.47	2.46±0.07	2.41±0.11	<0.01
Elongation	4.93±0.65	4.97±0.71	0.82	5.64±0.66	7.75±0.94	<0.01
Diameter (mm)	9.07±0.95	9.07±0.97	0.80	17.91±1.85	12.71±1.19	<0.01
Volume (mm ³)	2,902.43±709.96	2,938.5±799.94	0.84	25,422.3±5,280.07	12,460.97±2,267.12	<0.01
Trunk volume (mm ³)	1,403.97±518.6	1,339.93±589.23	0.54	9,928.5±5,916.96	5,553.83±2,439.64	<0.01
Branch volume (mm ³)	1,498.47±592.98	1,598.57±673.14	0.44	15,493.8±6,803.79	6,907.13±2,167.76	<0.01
Total surface area (mm ²)	8,004.53±1,487.61	8,180.53±1,544.64	0.73	48,918.57±7,768.94	27,238.03±4145	<0.01
Total radius of ER (mm ²)	12.78±0.98	12.47±1.22	0.41	34.69±6.93	21.74±2.84	<0.01
Total area of ER (mm ²)	515.17±100.36	494.83±101.79	0.09	3,242.63±650.21	1,714.9±370.65	<0.01
Irregularity	6.32±0.55	6.43±0.63	0.50	8.66±0.55	6.97±0.53	<0.01
Area of ER 1 (mm ²)	219.77±49.03	216.27±57.66	0.83	1,208.43±957.92	296.43±107.32	<0.01
Radius of ER 1 (mm)	7.5±1	7.23±1.19	0.22	14.71±9.82	7.36±1.15	<0.01
Irregularity of ER 1	0.87±0.3	0.81±0.3	0.67	0.66±0.6	0.67±0.31	0.46
QA	0.17±0.02	0.17±0.02	0.16	0.15±0.02	0.13±0.02	<0.01
NQA	0.3±0.03	0.3±0.02	0.20	0.26±0.02	0.24±0.02	<0.01
FA	0.39±0.03	0.39±0.03	0.22	0.43±0.02	0.41±0.02	<0.01
MD	1.33±0.13	1.27±0.14	0.05	0.88±0.04	0.86±0.04	0.13
AD	1.79±0.13	1.73±0.14	0.03	1.28±0.06	1.25±0.05	<0.01
RD	1.1±0.13	1.04±0.14	0.05	0.67±0.04	0.67±0.05	0.62

Data are shown as mean ± standard deviation. P<0.05 is considered statistically significant. ER, end region; QA, quantitative anisotropy; NQA, normalized quantitative anisotropy; FA, fractional anisotropy; MD, mean diffusivity; AD, axial diffusivity; RD, radial diffusivity.

The fibers connecting the cerebral cortex and the RN composed part of the reticular tracts. The RN set as an ROI in the reticular tract templates served as a filter that helped to accurately isolate the corticorubral tracts from the reticular tracts. Interestingly, most corticopontine tract fibers originated from the cortex that was scattered along the middle line of the parietal, frontal, and occipital lobes. Meanwhile, the corticorubral tracts mainly originated from the frontal lobe, especially from a part of the prefrontal cortex. The innervation area of these tracts was removed from the motor speech cortex, including the Broca area, and a considerable portion of them was located in the frontal lobe. This may indicate that the LRCCP and cerebellum

have more comprehensive roles in language function rather than simply in the coordination of the motor aspects of language function. The central tegmental tracts constituted a major fiber bundle in the brainstem, which included ascending axonal fibers and descending fibers. The rubroolivary tracts were part of the descending fibers (52). The key to obtaining an ideal tract was to accurately describe the outline of these 2 areas. The pontocerebellar tracts originated from the contralateral pontine nucleus and crossed the middle line to the contralateral cerebellum. A significant amount of dense parallel fibers formed at the ventral pontine. The algorithm that was applied could hardly dissect L- and R-side fibers in this area. This led

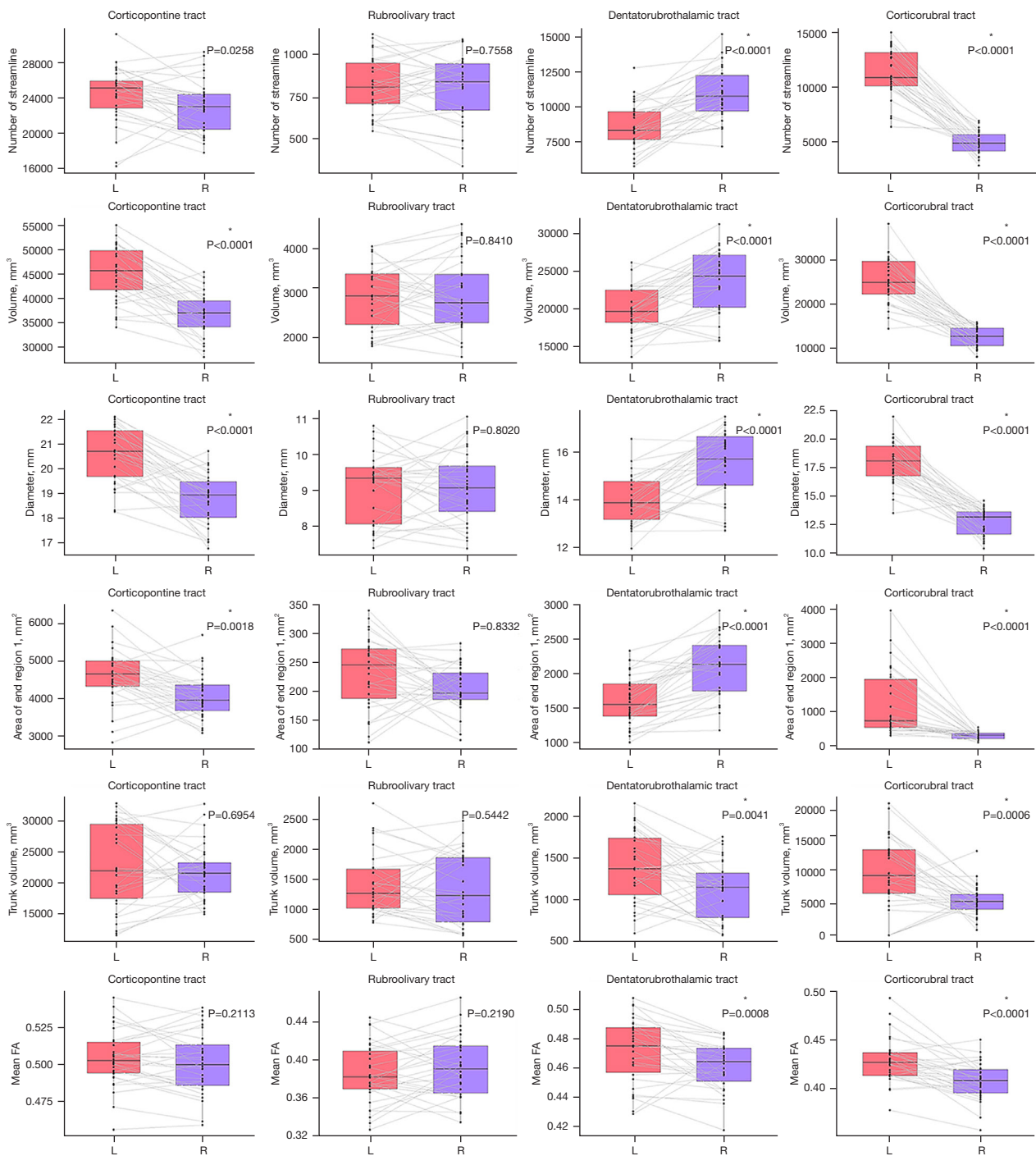


Figure 6 Paired box plot of the corticopontine, rubroolivary, dentatorubrothalamic, and corticorubral tracts showing the metrics of interest in the differences of white matter tracts. This figure shows the result of the comparison between the left hemisphere and right hemisphere with the paired *t* test. *, indicates that there is statistical difference (P<0.05). FA, fractional anisotropy.

to a greater value in volume and length, while the value of curl, span, and mean FA were generally inconsistent with the other tracts. The results of the pontocerebellar tracts verified the stability of the shape analysis methods, to some degree.

The shape analysis and LI of LRCCP

Diffusion metrics, such as FA, are known to be the most important measurement in the study of white matter (53). Nervous system diseases affecting the axon or myelin sheath are particularly suitable for this indicator (54). However, in other cases, such as regional congenital lesions or benign tumors with a long course, the specificity of diffusion metrics is lower compared to their applications in demyelinating and neurodegenerative diseases (15,27,55-57). It is hypothesized that cerebral lesions with a long history tend to result in few FA changes, especially in the indirectly connected white matter tract. The reason is that the brain has experienced eloquent remodeling of areas and adapted well to the lesion. In this scenario, shape analysis may perform better and provide a new direction for the study of the white matter tract (31,58). This method provides a set of parameters that describe in detail the shape characteristics of the white matter fiber bundles (31). The shape descriptors can be classified into length metrics, area metrics, volume metrics, and shape metrics. If a new cerebral cortex was recruited in the situation mentioned previously, a greater value would be observed in the innervation area, and vice versa. If a new tract were recruited, the “enhanced” fibers may exhibit changes in streamline number, tract volume, and even diameter. Changes in eloquent location may result in variations of shape metrics, such as curls. Metrics from native space can still provide valuable information while brain shape varies across different participants.

The lateralization pattern of cerebro-cerebellar activation in language function has been previously reported (59-61). The contralateral activation pattern is the most common type, and an ipsilateral activation pattern has also been reported (2,9). That both descending pathways from the cerebral cortex end in the contralateral cerebellum are consistent with anatomical fact. Both traverse the midline of the brainstem. In addition, the ascending pathway also contains partial fibers of DRTT that cross the midline to merge with the contralateral DRTT before entering the RN (41). Although there is no conclusive evidence that these fiber bundles are responsible

for language function, it is well accepted that this provides way for the cerebellum to participate in language functions. Therefore, for language-related research of the cerebellum, a comprehensive evaluation of this pathway is of great significance.

Similar to the dominant hemisphere in the human brain, previous research has also shown that white matter asymmetry exists in subcortical white matter fiber bundles (62). Most of the previous studies have focused on tract volume or the number of streamlines and FA (62,63). LI was derived from these indices to determine lateralization. The results of our study showed that white matter asymmetry of the cerebro-cerebellar pathway can also be observed in other metrics. For these healthy participants, the RT showed obvious leftward lateralization in most shape metrics and diffusion metrics. The DRTT showed rightward lateralization (*Figure 7*). The corticopontine tracts showed leftward lateralization in most shape analysis metrics except for the mean FA, while the rubroolivary tracts showed no difference in any shape analysis metrics or diffusion metrics. All tracts connected with the cerebral cortex showed varying degrees of lateralization. The rubroolivary tract is an internucleus fiber bundle with a relatively shorter route and more regular shape (41). In addition, the rubroolivary tracts are indirectly connected to the cerebral and cerebellum cortex. All these factors made it difficult to detect significant differences in shape metrics for the rubroolivary tracts. Rightward lateralization of the DRTT may be interpreted such that the DRTT connects the cerebral cortex and R cerebellum. According to the general principle of contralateral dominance in cerebral and cerebellar language function, the right cerebellum is thought to be the dominant hemisphere (64).

The corticorubral tracts are much smaller and topographically different in the R hemisphere compared with the L hemisphere. Generally speaking, such a difference in healthy participants is unexpected. As has been described in the method section, various factors affect the processing of the result of atlas recognition. The tractography result is fundamentally affected by the variations in the size of the seeding region and similar distance metrics. Most importantly, the TIP algorithm removes false streamlines which may eliminate some true fibers that do not meet the standard of “true fiber” in the algorithm. Further improvement of the algorithm and/or enlargement of the population size may help to achieve a better result but is beyond the scope of this paper.

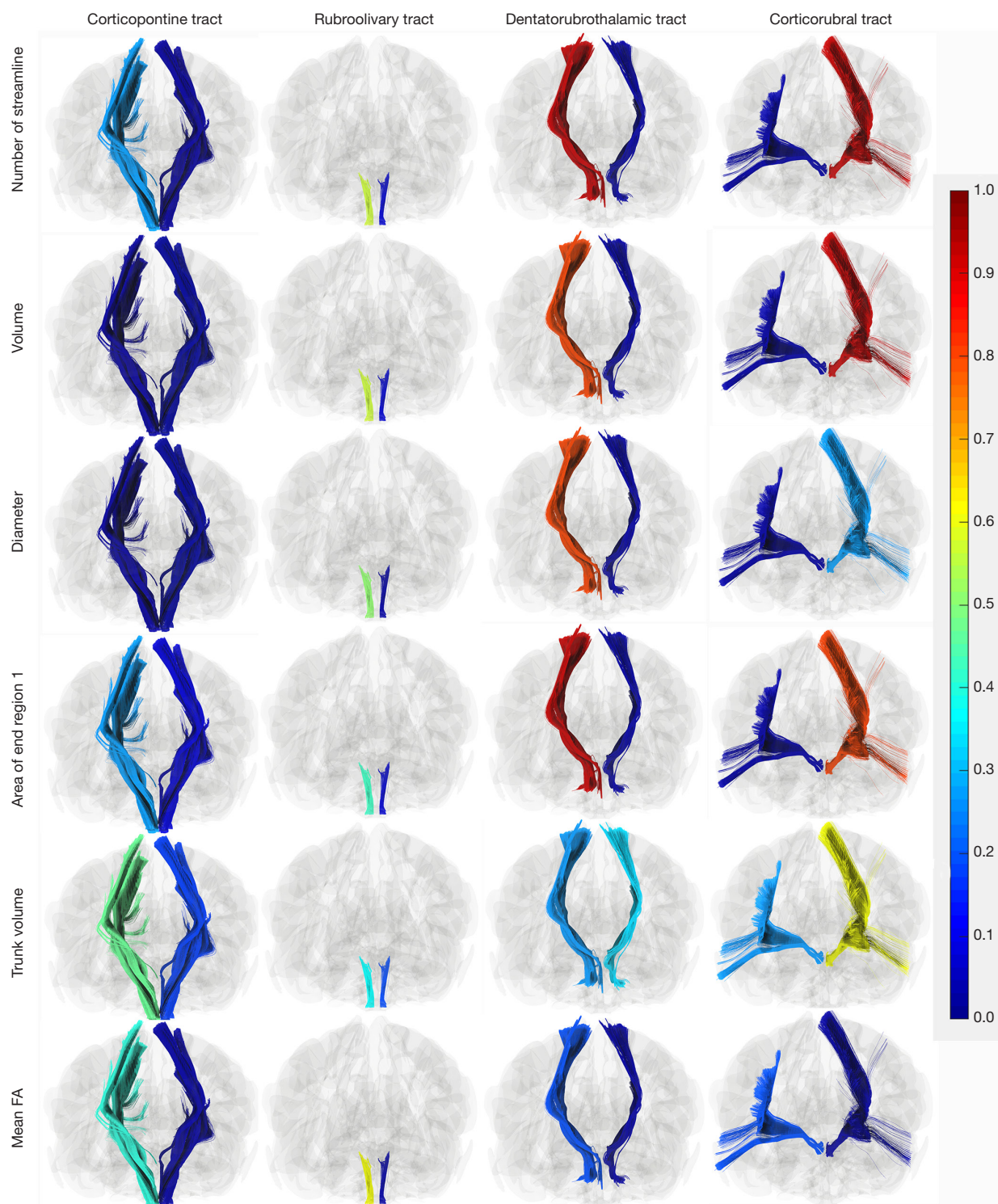


Figure 7 Lateralization index of metrics of interest in the corticopontine, rubroolivary, dentatorubrothalamic, and corticorubral tracts. The color of tracts corresponds with the percentage of participants with $LI > 0.2$ (left hemisphere) and $LI < 0$ (right hemisphere) in all participants. FA, fractional anisotropy; LI, lateralization index.

Limitations

There are several limitations to our work. First, the main caveat is that the language pathway is a concept that mainly focuses on function. Diffusion MRI studies provide morphological information based on this concept, which helps to determine the anatomic substance of this pathway. Hypotheses about the language pathway generally have no systematic and convincing evidence. fMRI studies and cases from clinical practice are mainly focused on cerebral eloquent and cerebellar regional differences. For the cerebellum, the most frequently mentioned language-related area is crus I and crus II in lobe VII (1). Studies that identify cerebro-cerebellar pathway white matter tracts related to language function are rare. DES may be the only method that allows direct verification of the function of the white matter tract. White matter tracts included in our study composed the main connection between the cerebellum and cerebrum. These white matter tracts represented the cerebro-cerebellar language pathway, to a certain degree. The second limitation of our study was that our newly built tractography template was based on the HCP datasets. All of the tracking results were based on the HCP 1065 (1 mm³), a population-averaged template. Thus, a tracking result for all healthy participants was produced, and all the quantities relied on the tracking result. The template and the tracking method might have omitted some obvious changes in the white matter tract in some situations when lesions or congenital variation was present. The third limitation was the limited number of participants in the study. A greater number of participants might have produced a more robust result regarding L- and R-side differences, and the trend of leftward lateralization might have been made clearer in the corticopontine tract.

Conclusions

Our study successfully built a set of tract templates of the cerebro-cerebellar pathway. A deterministic, fiber-tracking method in conjunction with the newly created templates was applied to obtain the diffusion and shape analysis metrics of healthy participants, acquired with lower resolution. We quantified these tracts in terms of diffusion and morphology. The mean FA values were generally consistent with previously reported values, demonstrating the feasibility of applying the LRCCP atlas to the datasets with clinical quality tracking studies. Shape analysis reflected the morphology of the tract accurately. This work

lays the foundation for further quantitative analysis of the LRCCP.

Acknowledgments

Funding: This study was supported by the Chinese National Natural Science Foundation (Nos. 81701088, 81870833, and 61901465), and the Beijing Talents Project (No. 2017000021469G211).

Footnote

Conflicts of Interest: All authors have completed the ICMJE uniform disclosure form (available at <https://qims.amegroups.com/article/view/10.21037/qims-22-303/coif>). The authors have no conflicts of interest to declare.

Ethical Statement: The authors are accountable for all aspects of the work in ensuring that questions related to the accuracy or integrity of any part of the work are appropriately investigated and resolved. The study was conducted in accordance with the Declaration of Helsinki (as revised in 2013). It was approved by the Institutional Review Board of Beijing Tiantan Hospital (number: KY2018-103-01) and registered in the Chinese Trial Registry (clinical trial number: ChiCTR1900020993). Written informed consent was obtained from all the enrolled participants.

Open Access Statement: This is an Open Access article distributed in accordance with the Creative Commons Attribution-NonCommercial-NoDerivs 4.0 International License (CC BY-NC-ND 4.0), which permits the non-commercial replication and distribution of the article with the strict proviso that no changes or edits are made and the original work is properly cited (including links to both the formal publication through the relevant DOI and the license). See: <https://creativecommons.org/licenses/by-nc-nd/4.0/>.

References

1. Murdoch BE. The cerebellum and language: historical perspective and review. *Cortex* 2010;46:858-68.
2. Mariën P, Borgatti R. Language and the cerebellum. *Handb Clin Neurol* 2018;154:181-202.
3. Leiner HC, Leiner AL, Dow RS. Cognitive and language functions of the human cerebellum. *Trends Neurosci* 1993;16:444-7.
4. Diedrichsen J, King M, Hernandez-Castillo C,

- Sereno M, Ivry RB. Universal Transform or Multiple Functionality? Understanding the Contribution of the Human Cerebellum across Task Domains. *Neuron* 2019;102:918-28.
5. Stoodley CJ, Schmahmann JD. The cerebellum and language: evidence from patients with cerebellar degeneration. *Brain Lang* 2009;110:149-53.
 6. Cui D, Zhang L, Zheng F, Wang H, Meng Q, Lu W, Liu Z, Yin T, Qiu J. Volumetric reduction of cerebellar lobules associated with memory decline across the adult lifespan. *Quant Imaging Med Surg* 2020;10:148-59.
 7. Stoodley CJ, Schmahmann JD. Functional topography in the human cerebellum: a meta-analysis of neuroimaging studies. *Neuroimage* 2009;44:489-501.
 8. Papanthassiou D, Etard O, Mellet E, Zago L, Mazoyer B, Tzourio-Mazoyer N. A common language network for comprehension and production: a contribution to the definition of language epicenters with PET. *Neuroimage* 2000;11:347-57.
 9. Cho NS, Peck KK, Zhang Z, Holodny AI. Paradoxical Activation in the Cerebellum During Language fMRI in Patients with Brain Tumors: Possible Explanations Based on Neurovascular Uncoupling and Functional Reorganization. *Cerebellum* 2018;17:286-93.
 10. Vias C, Dick AS. Cerebellar Contributions to Language in Typical and Atypical Development: A Review. *Dev Neuropsychol* 2017;42:404-21.
 11. Leiner HC, Leiner AL, Dow RS. Does the cerebellum contribute to mental skills? *Behav Neurosci* 1986;100:443-54.
 12. Leiner HC, Leiner AL, Dow RS. The human cerebro-cerebellar system: its computing, cognitive, and language skills. *Behav Brain Res* 1991;44:113-28.
 13. Balsters JH, Cussans E, Diedrichsen J, Phillips KA, Preuss TM, Rilling JK, Ramnani N. Evolution of the cerebellar cortex: the selective expansion of prefrontal-projecting cerebellar lobules. *Neuroimage* 2010;49:2045-52.
 14. Middleton FA, Strick PL. Anatomical evidence for cerebellar and basal ganglia involvement in higher cognitive function. *Science* 1994;266:458-61.
 15. Lidzba K, Wilke M, Staudt M, Krägeloh-Mann I, Grodd W. Reorganization of the cerebro-cerebellar network of language production in patients with congenital left-hemispheric brain lesions. *Brain Lang* 2008;106:204-10.
 16. Frings M, Dimitrova A, Schorn CF, Elles HG, Hein-Kropp C, Gizewski ER, Diener HC, Timmann D. Cerebellar involvement in verb generation: an fMRI study. *Neurosci Lett* 2006;409:19-23.
 17. Strick PL, Dum RP, Fiez JA. Cerebellum and nonmotor function. *Annu Rev Neurosci* 2009;32:413-34.
 18. Deng L, Liu H, Liu H, Liu J, Liu W, Liu Y, Zhang Y, Rong P, Liang Q, Wang W. Concomitant functional impairment and reorganization in the linkage between the cerebellum and default mode network in patients with type 2 diabetes mellitus. *Quant Imaging Med Surg* 2021;11:4310-20.
 19. Schmahmann JD. From movement to thought: anatomic substrates of the cerebellar contribution to cognitive processing. *Hum Brain Mapp* 1996;4:174-98.
 20. Bloedel JR, Bracha V. Duality of cerebellar motor and cognitive functions. *Int Rev Neurobiol* 1997;41:613-34.
 21. Palesi F, De Rinaldis A, Castellazzi G, Calamante F, Muhlert N, Chard D, Tournier JD, Mageses G, D'Angelo E, Gandini Wheeler-Kingshott CAM. Contralateral cortico-ponto-cerebellar pathways reconstruction in humans in vivo: implications for reciprocal cerebro-cerebellar structural connectivity in motor and non-motor areas. *Sci Rep* 2017;7:12841.
 22. Middleton FA, Strick PL. Dentate output channels: motor and cognitive components. *Prog Brain Res* 1997;114:553-66.
 23. Jbabdi S, Johansen-Berg H. Tractography: where do we go from here? *Brain Connect* 2011;1:169-83.
 24. Mori S, Zhang J. Principles of diffusion tensor imaging and its applications to basic neuroscience research. *Neuron* 2006;51:527-39.
 25. Negwer C, Sollmann N, Ille S, Hauck T, Maurer S, Kirschke JS, Ringel F, Meyer B, Krieg SM. Language pathway tracking: comparing nTMS-based DTI fiber tracking with a cubic ROIs-based protocol. *J Neurosurg* 2017;126:1006-14.
 26. Keser Z, Hasan KM, Mwangi BI, Kamali A, Ucisik-Keser FE, Riascos RF, Yozbatiran N, Francisco GE, Narayana PA. Diffusion tensor imaging of the human cerebellar pathways and their interplay with cerebral macrostructure. *Front Neuroanat* 2015;9:41.
 27. Zhang N, Xia M, Qiu T, Wang X, Lin CP, Guo Q, Lu J, Wu Q, Zhuang D, Yu Z, Gong F, Farrukh Hameed NU, He Y, Wu J, Zhou L. Reorganization of cerebro-cerebellar circuit in patients with left hemispheric gliomas involving language network: A combined structural and resting-state functional MRI study. *Hum Brain Mapp* 2018;39:4802-19.
 28. Glasser MF, Rilling JK. DTI tractography of the human brain's language pathways. *Cereb Cortex* 2008;18:2471-82.
 29. Van Essen DC, Smith SM, Barch DM, Behrens TE,

- Yacoub E, Ugurbil K; . The WU-Minn Human Connectome Project: an overview. *Neuroimage* 2013;80:62-79.
30. Yeh FC, Panesar S, Fernandes D, Meola A, Yoshino M, Fernandez-Miranda JC, Vettel JM, Verstynen T. Population-averaged atlas of the macroscale human structural connectome and its network topology. *Neuroimage* 2018;178:57-68.
 31. Yeh FC. Shape analysis of the human association pathways. *Neuroimage* 2020;223:117329.
 32. Yeh FC, Verstynen TD, Wang Y, Fernández-Miranda JC, Tseng WY. Deterministic diffusion fiber tracking improved by quantitative anisotropy. *PLoS One* 2013;8:e80713.
 33. Yeh FC, Tseng WY. NTU-90: a high angular resolution brain atlas constructed by q-space diffeomorphic reconstruction. *Neuroimage* 2011;58:91-9.
 34. Yeh FC, Wedeen VJ, Tseng WY. Generalized q-sampling imaging. *IEEE Trans Med Imaging* 2010;29:1626-35.
 35. Yeh FC, Panesar S, Barrios J, Fernandes D, Abhinav K, Meola A, Fernandez-Miranda JC. Automatic Removal of False Connections in Diffusion MRI Tractography Using Topology-Informed Pruning (TIP). *Neurotherapeutics* 2019;16:52-8.
 36. Deng X, Yin H, Zhang Y, Zhang D, Wang S, Cao Y, Li M, Wang B, Zong F, Zhao J. Impairment and Plasticity of Language-Related White Matter in Patients With Brain Arteriovenous Malformations. *Stroke* 2022;53:1682-91.
 37. Mannaert L, Verhelst H, Gerrits R, Bogaert S, Vingerhoets G. White matter asymmetries in human situs inversus totalis. *Brain Struct Funct* 2019;224:2559-65.
 38. O'Muircheartaigh J, Dean DC 3rd, Dirks H, Waskiewicz N, Lehman K, Jerskey BA, Deoni SC. Interactions between white matter asymmetry and language during neurodevelopment. *J Neurosci* 2013;33:16170-7.
 39. Joo SW, Chon MW, Rathi Y, Shenton ME, Kubicki M, Lee J. Abnormal asymmetry of white matter tracts between ventral posterior cingulate cortex and middle temporal gyrus in recent-onset schizophrenia. *Schizophr Res* 2018;192:159-66.
 40. Fujita H, Sugihara I. Branching patterns of olivocerebellar axons in relation to the compartmental organization of the cerebellum. *Front Neural Circuits* 2013;7:3.
 41. Haines DE, Dietrichs E. The cerebellum - structure and connections. *Handb Clin Neurol* 2012;103:3-36.
 42. Reeber SL, White JJ, George-Jones NA, Sillitoe RV. Architecture and development of olivocerebellar circuit topography. *Front Neural Circuits* 2013;6:115.
 43. Habas C, Guillevin R, Abanou A. In vivo structural and functional imaging of the human rubral and inferior olivary nuclei: A mini-review. *Cerebellum* 2010;9:167-73.
 44. Gruol, DL, Koibuchi N, Manto M, Molinari M, Schmahmann JD, Shen Y. *Essentials of Cerebellum and Cerebellar Disorders*. Springer; 2016.
 45. Sugihara I, Wu H, Shinoda Y. Morphology of single olivocerebellar axons labeled with biotinylated dextran amine in the rat. *J Comp Neurol* 1999;414:131-48.
 46. Naidich TP, Duvernoy HM, Delman BN, Sorensen AG, Kollias SS, Haacke EM. *Duvernoy's Atlas of the Human Brain Stem and Cerebellum*. Springer; 2009.
 47. Voogd J, Ruigrok TJH. *Cerebellum and Precerebellar Nuclei*. In: Mai JK, Paxinos G. editors. *The Human Nervous System*. 2012;471-545.
 48. Tang Y, Sun W, Toga AW, Ringman JM, Shi Y. A probabilistic atlas of human brainstem pathways based on connectome imaging data. *Neuroimage* 2018;169:227-39.
 49. Wang F, Dong Z, Tian Q, Liao C, Fan Q, Hoge WS, Keil B, Polimeni JR, Wald LL, Huang SY, Setsompop K. In vivo human whole-brain Connectom diffusion MRI dataset at 760µm isotropic resolution. *Sci Data* 2021;8:122.
 50. Re TJ, Levman J, Lim AR, Righini A, Grant PE, Takahashi E. High-angular resolution diffusion imaging tractography of cerebellar pathways from newborns to young adults. *Brain Behav* 2016;7:e00589.
 51. Schilling KG, Petit L, Rheault F, Remedios S, Pierpaoli C, Anderson AW, Landman BA, Descoteaux M. Brain connections derived from diffusion MRI tractography can be highly anatomically accurate-if we know where white matter pathways start, where they end, and where they do not go. *Brain Struct Funct* 2020;225:2387-402.
 52. Kamali A, Kramer LA, Butler IJ, Hasan KM. Diffusion tensor tractography of the somatosensory system in the human brainstem: initial findings using high isotropic spatial resolution at 3.0 T. *Eur Radiol* 2009;19:1480-8.
 53. Assaf Y, Pasternak O. Diffusion tensor imaging (DTI)-based white matter mapping in brain research: a review. *J Mol Neurosci* 2008;34:51-61.
 54. Filippi M, Agosta F. Diffusion tensor imaging and functional MRI. *Handb Clin Neurol* 2016;136:1065-87.
 55. Zhang H, Schramm S, Schröder A, Zimmer C, Meyer B, Krieg SM, Sollmann N. Function-Based Tractography of the Language Network Correlates with Aphasia in Patients with Language-Eloquent Glioblastoma. *Brain Sci* 2020.
 56. Verhoeven JS, Rommel N, Prodi E, Leemans A, Zink I, Vandewalle E, Noens I, Wagemans J, Steyaert J, Boets B, Van de Winckel A, De Cock P, Lagae L, Sunaert S. Is there a common neuroanatomical substrate of language

- deficit between autism spectrum disorder and specific language impairment? *Cereb Cortex* 2012;22:2263–71.
57. D'Mello AM, Stoodley CJ. Cerebro-cerebellar circuits in autism spectrum disorder. *Front Neurosci* 2015;9:408.
58. Speckter H, Bido J, Hernandez G, Rivera D, Suazo L, Valenzuela S, Miches I, Oviedo J, Gonzalez C, Stoeter P. Pretreatment texture analysis of routine MR images and shape analysis of the diffusion tensor for prediction of volumetric response after radiosurgery for meningioma. *J Neurosurg* 2018;129:31–7.
59. Knecht S, Dräger B, Deppe M, Bobe L, Lohmann H, Flöel A, Ringelstein EB, Henningsen H. Handedness and hemispheric language dominance in healthy humans. *Brain* 2000;123 Pt 12:2512–8.
60. Mariën P, Paghiera B, De Deyn PP, Vignolo LA. Adult crossed aphasia in dextrals revisited. *Cortex* 2004;40:41–74.
61. Johnsen SD, Bodensteiner JB, Lotze TE. Frequency and nature of cerebellar injury in the extremely premature survivor with cerebral palsy. *J Child Neurol* 2005;20:60–4.
62. Barrick TR, Lawes IN, Mackay CE, Clark CA. White matter pathway asymmetry underlies functional lateralization. *Cereb Cortex* 2007;17:591–8.
63. Büchel C, Raedler T, Sommer M, Sach M, Weiller C, Koch MA. White matter asymmetry in the human brain: a diffusion tensor MRI study. *Cereb Cortex* 2004;14:945–51.
64. Marien P, Engelborghs S, Fabbro F, De Deyn PP. The lateralized linguistic cerebellum: a review and a new hypothesis. *Brain Lang* 2001;79:580–600.

Cite this article as: Yin H, Zong F, Deng X, Zhang D, Zhang Y, Wang S, Wang Y, Zhao J. The language-related cerebro-cerebellar pathway in humans: a diffusion imaging–based tractographic study. *Quant Imaging Med Surg* 2023;13(3):1399–1416. doi: 10.21037/qims-22-303